PAPER

Check for updates

Novel alginate nanoparticles for the simultaneous delivery of iron and folate: a potential nano-drug delivery system for anaemic patients

Weranga Rajapaksha, [ID] *[a] Irosha H. W. Nicholas,[a,b] T. Thoradeniya,[c]
D. Nedra Karunaratne*[d] and V. Karunaratne[a,d,e]

Biopolymer nanoparticles have emerged as promising carriers for bioactive agents, offering sustained or controlled release and improved biocompatibility. The purpose of this study was to design novel calcium cross-linked alginate nanoparticles as a delivery system for ferrous ascorbate and folic acid, synthesized through a modified ionic gelation method, to enhance their oral bioavailability. Calcium alginate nanoparticles were successfully prepared using a modified ionic gelation method, and their particle size and zeta potential were characterized. These nanoparticles were then loaded with ferrous ascorbate and folic acid, and successful encapsulation was confirmed using electron energy loss spectroscopy (EELS) and X-ray photoelectron spectroscopy (XPS). The morphology of the loaded nanoparticles was also investigated using electron microscopy techniques. The encapsulation efficiency of ferrous ascorbate and folic acid was determined to be $95 \pm 1.9\%$ and $80 \pm 0.7\%$, respectively. *In vitro* release studies demonstrated that the release of ferrous ascorbate and folic acid from the loaded nanoparticles was pH-dependent, with a slower release rate being observed at pH 7.4 compared to that at pH 2. The release kinetics was found to follow the Korsmeyer–Peppas diffusion model, suggesting a combination of Fickian diffusion and anomalous diffusion mechanisms. Overall, the findings of this study indicate that the alginate nanoparticles have the potential to serve as a promising nano-drug delivery system for ferrous ascorbate and folic acid, potentially improving their oral bioavailability and therapeutic efficacy in the treatment and prevention of anaemia.

1. Introduction

Iron and folate are two essential trace elements for human health, especially for pregnant women and children.[1] Iron deficiency is the most common nutritional problem worldwide, causing anaemia and other health consequences, such as weakness, fatigue, adverse pregnancy outcomes, and impaired cognitive development.[2] Folate deficiency can also lead to anaemia, as well as neural tube defects and foetal growth retardation.[3,4] The main causes of iron and folate deficiency are blood loss, low dietary intake, poor absorption, and increased demand during pregnancy.[5,6] The absorption of iron and folate can be affected by various factors, such as ascorbic acid, dietary inhibitors, and pH.[7]

Iron and folate deficiencies can be effectively addressed by encapsulating these elements within a nano-drug delivery system, such as alginate nanoparticles (NPs), shielding them from degradation and unfavourable interactions within the harsh gastrointestinal environment.[8] The nano-drug delivery system encapsulates the drugs, protecting them from other substances that hinder absorption. This enhances their bioavailability and solubility, eliminating the need for high-dose intake.[9] Encapsulation within this system further offers the benefit of reduced side effects and toxicity associated with high doses, making it a promising therapeutic approach.[10] Additionally, nanoformulations improve patient compliance and convenience by enabling controlled and sustained release of drugs.[11] This slow-release ability of the drug from the nanoparticle matrix effectively minimizes side effects and allows for precise dosage control.[12]

Alginate possesses excellent properties for developing a nano-drug delivery system for ferrous and folic acid. It is a natural polysaccharide derived from brown algae, which has

*[a]Sri Lanka Institute of Nanotechnology, Mahenwatta, Pitipana, Homagama,
Sri Lanka. E-mail: Weranga.r2@gmail.com*

[b]Faculty of Medicine, Sabaragamuwa University, Sri Lanka

*[c]Department of Biochemistry and Molecular Biology, Faculty of Medicine,
University of Colombo, Sri Lanka*

*[d]Department of Chemistry, Faculty of Science, University of Peradeniya, Peradeniya,
Sri Lanka. E-mail: nedrak@pdn.ac.lk*

[e]SLTC Research University, Padukka, Sri Lanka

various applications in the pharmaceutical and biomedical fields.[13] Alginate is biocompatible, biodegradable, and non-toxic, and can form stable and viscous solutions in water.[14] Alginate can also undergo sol–gel transition under mild conditions, by interacting with divalent cations, such as calcium.[15] It can form hydrogels with different properties and structures, depending on the alginate composition and concentration.[16] Alginate hydrogels have diverse applications, including drug delivery, tissue engineering, and wound healing.[17] For instance, Katuwavila *et al.* successfully synthesized ferrous-encapsulated alginate nanoparticles with 75% encapsulation efficiency.[18] Additionally, folic acid encapsulation in alginate–pectin nanoparticles demonstrated promising pH-sensitive controlled release with 70% encapsulation efficiency.[19] This study aims to develop iron and folic acid encapsulated in novel alginate-based nanoformulations specifically for oral delivery and evaluate the release properties of drugs under variable pH conditions.

2. Materials and methods

This section discusses the synthetic procedures, materials, and methods used for nanoparticle synthesis and characterisation.

2.1. Materials

Sodium alginate (low molecular weight), calcium chloride, L-ascorbic acid, folic acid, ferrous ammonium sulphate hexahydrate, hydrochloric acid, sodium hydroxide, ammonium hydroxide, Span 20, potassium chloride, sodium chloride, sodium dihydrogen phosphate, sodium hydrogen phosphate, and potassium dihydrogen phosphate were purchased from Sigma-Aldrich, USA. All chemicals were of analytical grade. SnakeSkin™ dialysis membrane (molecular weight cut-off 3.5 kDa) was purchased from Thermo Scientific, USA.

2.2. Synthesis of calcium cross-linked alginate nanoparticles

Alginate NPs were prepared using a modified ionic gelation method. The pH of a 0.3% w/v solution of sodium alginate (20.0 mL) was adjusted to around six and then stirred with 0.5 mL of Span 20 for 1 h at 60 °C to obtain a homogeneous mixture. The above mixture was cross-linked by dropwise addition to 20.0 mL of $CaCl_2$ solution (0.05% w/v), using a 22-gauge needle while stirring at 1800 rpm. A drop rate of 1.0 mL per minute was maintained using a syringe pump (Thermo Scientific, Fusion T100). The suspension of NPs was refrigerated overnight and centrifuged (Beckman Coulter Inc., 64R, USA) at 10 000 rpm for 30 min to obtain NP pellets. The resulting NP pellets were washed with deionized water. Both NPs and supernatants were stored at 4 °C for further analysis.[18]

2.2.1. Ferrous ascorbate and folic acid encapsulation. A ferrous ammonium sulphate solution (1.0 mL) of a 3% w/v stock solution in the presence of ascorbic acid was stirred with Span 20 and the alginate mixture mentioned above. The mass ratio of ferrous ammonium sulphate to ascorbic acid was

maintained at 15 : 1 at varying concentrations of 0.5%, 1%, and 2% w/w alginate. A folic acid stock solution (1.0 mL of 0.06% (w/v)) was stirred with the Span 20 and alginate mixture for 30 minutes. Folic acid stock solution (0.06% w/v) was prepared by dissolving 60 mg of folic acid in 100 mL of distilled water and 1 mL of 3 M ammonium hydroxide. Various concentrations were used for encapsulation.

2.3. Characterization of ferrous ascorbate and folic acid loaded alginate NPs

2.3.1. Particle size analysis and zeta potential measurement. Measurements of the average size, polydispersity index (PDI) and zeta potential of the alginate NPs were determined by dynamic light scattering at 25 °C using a Zetasizer instrument (Nano-ZS, ZEN 3600, Malvern Instruments, Malvern, UK) at a fixed scattering angle of 173°.

2.3.2. Fourier transform infrared spectroscopy analysis. Fourier transform infrared spectroscopy analysis (FT-IR) analysis of blank alginate NPs and ferrous ascorbate and folic acid loaded calcium alginate NPs was performed using an FT-IR spectrometer (Bruker Vertex 80, Germany) operated with a resolution of 4 cm^{-1} and 64 scans across a frequency range of 400 to 4000 cm^{-1}. Samples were analyzed in the attenuated total reflectance (ATR) mode.

2.3.3. Scanning electron microscopy. The morphology of alginate NPs was examined by scanning electron microscopy (SEM, SU6600, Hitachi, Japan) at an accelerating voltage of 10 kV and ×80.0k magnification. A drop each of the blank alginate NP suspension and ferrous ascorbate and folic acid loaded alginate NP suspensions were separately mounted on a metal stub covered with a double-sided carbon adhesive disc. This metal stub was allowed to dry at room temperature, sputter-coated with gold and then imaged using SEM.

2.3.4. Transmission electron microscopy. A 1 microliter drop of ferrous ascorbate and folic acid loaded alginate NP suspension was placed on a holey carbon Cu grid and allowed to dry at room temperature. The particles were imaged using a high-resolution transmission electron microscope (TEM) (JEM 2100, JEOL, Japan) operated at an accelerating voltage of 200 kV.

2.3.5. Electron energy loss spectroscopy (EELS) analysis. EELS spectra of ferrous ascorbate and folic acid loaded alginate NPs were obtained with an EELS spectrometer (EELS Gatan, Quantum 963, USA) attached to the TEM with an energy resolution of 0.05 eV per channel in the STEM spectral imaging mode. EELS spectra of ferrous ascorbate and folic acid loaded alginate NPs and XPS analysis data were used for a comparative study.

2.3.6. X-ray photoelectron spectroscopy analysis. X-ray photoelectron spectroscopy (XPS) was performed using a photoelectron spectrometer incorporating a 165 mm EXCALABXi + hemispherical electron energy analyzer (Thermo Fisher Scientific, USA). The incident radiation was monochromatic Al Kα X-rays (1486.6 eV). Thermo Avantage (5.982) software was used for data acquisition and processing, including curve-fitting. All binding energies were referenced by setting

the C 1s peak to 284.8 eV; this component corresponds to carbon in a hydrocarbon environment. Component energies, number of peaks, and peak widths (full width at half maximum of 1.0 for all C 1s peaks) were fixed initially and refinement was carried out only for peak heights.

2.3.7. Thermogravimetric analysis. Thermal decomposition of blank alginate NPs, ferrous ascorbate and folic acid loaded calcium alginate NPs were analyzed using an SDT Q600 thermogravimetric analyzer (TA Instruments, USA). An appropriate amount of sample (5–10 mg) was placed onto a standard alumina pan and heated from 25 °C to 1000 °C under a nitrogen environment (at a flow rate of 100 mL min^{-1}) at a constant heating rate of 10 °C min^{-1}.

2.4. Encapsulation efficiency and loading capacity

The amount of encapsulated folic acid in the NPs was determined using a UV-visible spectrophotometer. The absorbance of folic acid was measured at 281 nm using a UV-vis spectrophotometer (SHIMADZU, UV-3600, UV-vis-NIR). Distilled water was used as the blank. The NP suspension was obtained after centrifugation and hydrogel was dissolved to remove the entrapped folic acid from the NPs. The solution was subjected to UV-vis spectrophotometric analysis. Another sample of NP suspension was centrifuged, and the precipitated hydrogel was freeze-dried to remove water. Then, the concentration was calculated from a calibration plot obtained for the folic acid standard solution. The percentage encapsulation efficiency (EE, %) and loading capacity (LC, %) were calculated as follows:[20]

$$EE = \frac{amount_{encapsulated}}{amount_{total}} \times 100\%$$

$$LC = \frac{amount_{encapsulated}}{weight\ of\ precipitated\ NPs} \times 100\%$$

The hydrogel pellets obtained after centrifugation were redissolved in distilled water and the solution was subjected to iron quantification. The amount of iron in the NPs was determined using an inductively coupled plasma mass spectrometer (ICP-MS). The ICP-MS (Agilent 7900 ICP-MS system – Agilent Technologies, USA) was operated in the Ar gas mode for iron to reduce polyatomic interferences caused by the plasma gas, reagents, and the sample matrix. The percentages of encapsulation efficiency and loading capacity were calculated.

2.5. *In vitro* release study of ferrous ascorbate–folic acid loaded alginate nanoparticles

The release behaviour of ferrous ascorbate and folic acid loaded alginate NPs was evaluated in pH 7.4 (PBS; phosphate-buffered saline) and pH 2 buffer solutions. A 5.00 g hydrogel of ferrous ascorbate–folic acid loaded alginate NPs was placed into a dialysis sac (molecular weight cut-off 3000 kDa) containing 10.00 mL of the buffer solution. The enclosed dialysis bag was immersed in a beaker containing the pH 2 buffer solutions at 37 °C with mild agitation (100 rpm) for the first 3.5 hours. For each sample, a 3.00 mL aliquot of the dialysate

was withdrawn at predetermined time intervals and replaced by the same medium under the same conditions. After 3.5 hours, the dialysis sac was removed and immersed in a beaker containing the pH 7.4 buffer solutions at 37 °C with mild agitation (100 rpm) for 6 hours. The released amount of ferrous ascorbate and folic acid was quantified using ICP-MS and UV-visible spectrophotometry as described above. All measurements were performed in triplicate. The cumulative drug release percentages were calculated and plotted against time.

2.6. Kinetics analysis

Release data obtained from the *in vitro* release studies were fitted to 5 different mathematical models, namely zero order, first order, Higuchi, Korsmeyer–Peppas and Hixson–Crowell, as described by Siepmann and Peppas (2001) to evaluate the release profile of ferrous ascorbate and folic acid from alginate NPs.[21] The optimum model was selected based on the correlation coefficient value (r^2) of various models. Furthermore, the first 60% of drug release data were fitted in the Korsmeyer–Peppas model to evaluate the mechanism of drug release.

3. Results and discussion, experimental

3.1. Preparation of calcium cross-linked alginate nanoparticles

Calcium cross-linked alginate NPs were synthesized using a modified ionic gelation method. In this technique, calcium was used as divalent cations for the synthesis of uniform alginate NPs. The basic concept of this developed drug delivery system is based on the special characteristic feature of sodium alginate, that it becomes a gel-like structure in the presence of a divalent metal ion. In molecular terms, alginate is a family of unbranched binary copolymers, consisting of homopolymeric regions of mannuronic acid (M) and guluronic acid (G). Alginate behaves like flexible coils in an aqueous solution. However, alginate is converted into an ordered structure called an egg-box model upon interaction with divalent metal ions such as calcium. In this study, a ferrous ascorbate complex and folic acid were added to the alginate solution for entrapment during the formation of NPs and a hydrogel. This cross-linking occurs spontaneously *via* the electrostatic interactions between the negatively charged carboxylate groups on the alginate and the positively charged calcium ions.

3.2. Determination of the particle size and surface charge

3.2.1. Effect of cross-linker concentration on the particle size and zeta potential of alginate nanoparticles. The size and zeta potential of the NPs play an important role in their mechanism of cellular uptake and the stability of NP suspensions. Particles with diameters of 60–100 nm have been proven to have the best properties for cellular uptake in previous studies, with a range of 100 nm indicated as the ideal size.[22]

In this study, it was observed that the size and zeta potential were strongly dependent on the amount of alginate and the cross-linker concentration (Fig. 1a). When increasing the cross-linker concentration while keeping the alginate concentration constant, the size of NPs increases (Table 1). The minimum average size of 66 ± 0.8 nm corresponds to the lowest calcium chloride concentration (0.05% w/v) and the maximum average size, $6 \times 10^5 \pm 0.0$ nm, corresponds to the highest calcium chloride concentration (0.5% w/v). These

results confirm that smaller NPs result when the ability of the interactions between functional groups of the polymer and the cross-linker is reduced by smaller stoichiometric proportions. Since a PDI value of 1 is indicative of different size distributions, we have used the concentrations where the PDI is below 1 to ensure our preparations are of uniform size.

On the other hand, the zeta potential of the NPs was affected by the concentration of the cross-linker. The negative value of the zeta potential was increased from −12 ± 0.2 mV to −31 ± 1.1 mV when the cross-linker concentration was decreased from 0.5% to 0.05%, respectively (Fig. 1a). This result could be due to the increase in the ratio of negatively charged carboxylate groups to the cross-linker cations with increasing cross-linker concentration. This higher electric charge on the surface of the NPs can produce strong repulsive forces among adjacent NPs to prevent their aggregation in solution. So, the particles are considered as stable. Particles tend to aggregate when the cross-linker concentration increases due to the reduction of the zeta potential of the NPs (Fig. 1b).

Particle size analysis and zeta potential results are summarized in Table 1. The mean size of optimized blank alginate NPs was 66 ± 0.8 nm, and the zeta potential was −31 ± 1.1 mV. When encapsulating both ferrous ascorbate and folic acid into the calcium alginate NPs, the size was increased to 76 ± 2.1 nm with a zeta potential of −28 ± 2.1 mV (Table 2).

According to the particle size analysis results summarized in Tables 2 and 3, the encapsulation of ferrous ascorbate and folic acid into the NPs has a significant influence ($p < 0.05$) on the average size of the alginate NPs. However, the zeta potential is inversely proportional to the concentration of the ferrous ascorbate. Increasing the ferrous ascorbate concentration decreases the zeta potential of the alginate NPs: a tendency towards particle aggregation was also observed. According to the results in Table 3, increasing the ferrous ascorbate concentration from 0.05 to 0.2%, decreased the zeta potential from −27 ± 0.6 mV to −21 ± 0.6 mV and increased the particle size because the solution became acidic. However, with increased encapsulation of folic acid into the NPs, an increase in the size of the NPs was observed. At the same time, the NPs become stabilized due to the increment of the zeta potential (Fig. 2a and b).

3.2.2. Effect of pH on the particle size. The effect of pH on the size and zeta potential of alginate NPs was observed. According to the data summarized in Table 4, pH 6 was the most ideal for NP synthesis since small size, high encapsulation efficiency and loading capacity (Table 8) were observed at pH 6. The carboxyl groups of the alginate are ionized at pH 6, which is most important for the interaction of the alginate and the cross-linker. The pK_a values of alginate's mannuronic acid and guluronic acid blocks are 3.38 and 3.65, respectively.[23] When the pH of alginate drops below these pK_a values, it starts to precipitate and becomes stabilized by an intermolecular hydrogen bonding network. Hence, alginate NPs are stable in gastric juice and are easily disintegrated in intestinal juice due to the pH difference.[24,25]
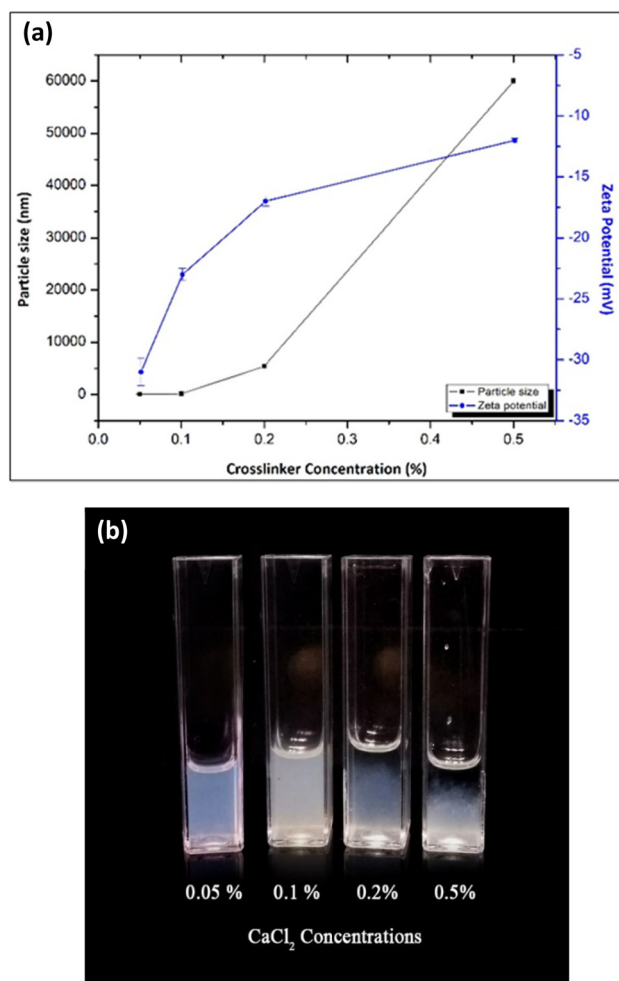

Fig. 1 (a) Effect of cross-linker on the particle size and zeta potential and (b) particle aggregation with cross-linker concentration.

Table 1 Summary of particle size analysis results with different conditions ($n = 3$, ±SEM)

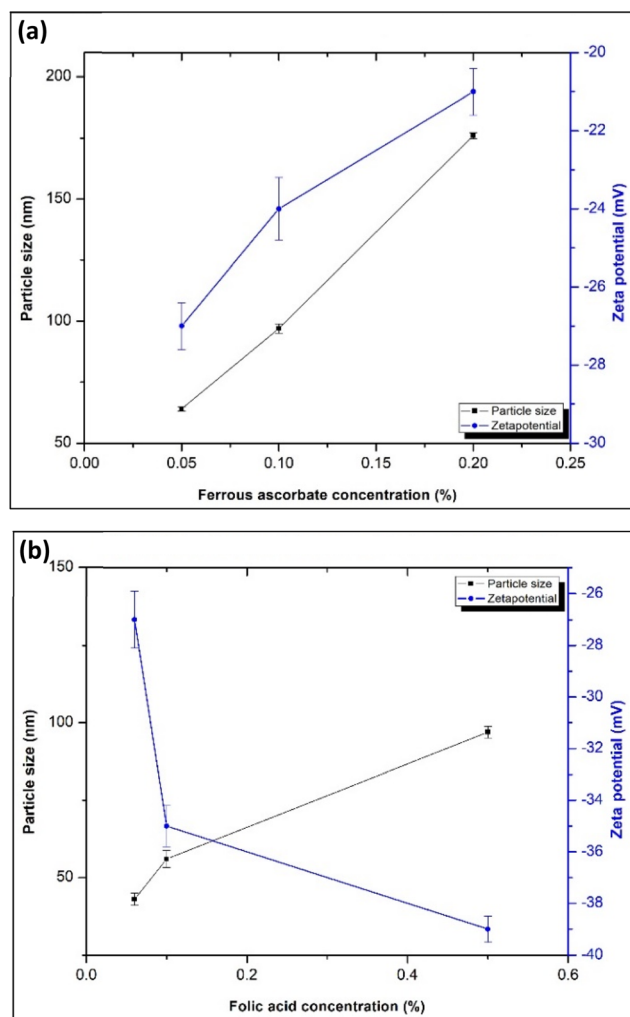| Alginate concentration (pH 5)	CaCl$_2$ concentration	Particle size (nm)	PDI	Zeta potential (mV)
0.3%	0.5%	$6 \times 10^4 \pm 0.0$	1.000	−12 ± 0.2
0.3%	0.2%	5445 ± 0.0	1.000	−17 ± 0.4
0.3%	0.1%	164 ± 0.0	0.343	−23 ± 0.5
0.3%	0.05%	66 ± 0.8	0.245	−31 ± 1.1

Table 2 Summary of dynamic light scattering analysis results ($n = 3$, $\pm$SEM)

	Particle size	PDI	Zeta potential
Blank calcium alginate NPs	66 ± 0.8 nm	0.245	−31 ± 1.1 mV
Ferrous ascorbate and folic acid loaded calcium alginate NPs	76 ± 2.1 nm	0.203	−28 ± 2.1 mV

Table 3 Summary of particle size analysis results of encapsulated calcium alginate nanoparticles ($n = 3$, $\pm$SEM)

	Ferrous ascorbate concentration			Folic acid concentration		
	0.05%	0.1%	0.2%	0.06%	0.1%	0.5%
Particle size (nm)	64 ± 0.9	97 ± 1.9	176 ± 1.3	43 ± 2.0	56 ± 2.7	97 ± 1.9
Zeta potential (mV)	−27 ± 0.6	−24 ± 0.8	−21 ± 0.6	−27 ± 1.1	−35 ± 0.8	−39 ± 0.5
PDI	0.248	0.264	0.233	0.244	0.238	0.223

Fig. 2 (a) Effect of ferrous ascorbate concentration and (b) effect of folic acid concentration on the size and zeta potential of alginate nanoparticles.

However, this precipitation and aggregation of alginate leads to increased particle size and a decrease in encapsulation efficiency.

Table 4 Effect of pH on the size and zeta potential of nanoparticles obtained ($n = 3$, $\pm$SEM)

The pH of nanoparticle formulation	Size (nm) of the calcium alginate NPs	Zeta potential (mV) of the calcium alginate NPs	PDI
5	66 ± 0.8	−31 ± 1.1	0.245
6	53 ± 2.7	−30 ± 1.2	0.225
7	38 ± 3.2	−34 ± 0.0	0.239

3.3. Characterization of ferrous ascorbate and folic acid loaded alginate NPs

The morphology of ferrous ascorbate and folic acid loaded alginate NPs was observed using a scanning electron microscope and a transmission electron microscope.

3.3.1. Scanning electron microscopy (SEM). The morphology of the prepared blank alginate NPs and ferrous ascorbate/folic acid loaded alginate NPs was observed using SEM and respective images are shown in Fig. 3(a) and (b). They exhibit spherical-shaped particles embedded in a sheet-like structure. The average size of the spherical structures in the blank calcium alginate NP suspension and the ferrous ascorbate/folic acid loaded calcium alginate NP suspension was approximately 60 to 80 nm.

3.3.2. Transmission electron microscopy (TEM). The alginate NP suspension was further characterized by transmission electron microscopy, as shown in Fig. 4. The spherically distinct 15 nm alginate NPs were observed to lie between thin film-like structures.

The observed discrepancy in nanoparticle size between dynamic light scattering (DLS), SEM, and TEM analysis can be attributed to the fundamental differences in the techniques. DLS measures the hydrodynamic diameter, reflecting the size of NPs with their surrounding hydration layer in solution. In contrast, SEM and TEM visualize the dry state morphology, capturing the particle core size. During sample preparation for SEM and TEM, drying steps can induce shrinkage, leading to smaller dimensions compared to the hydrated particles measured by DLS.
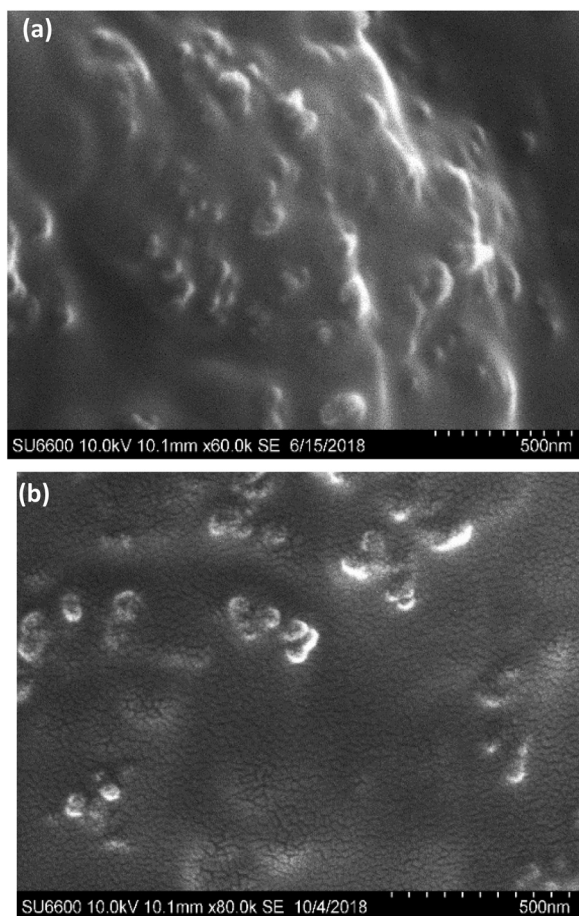
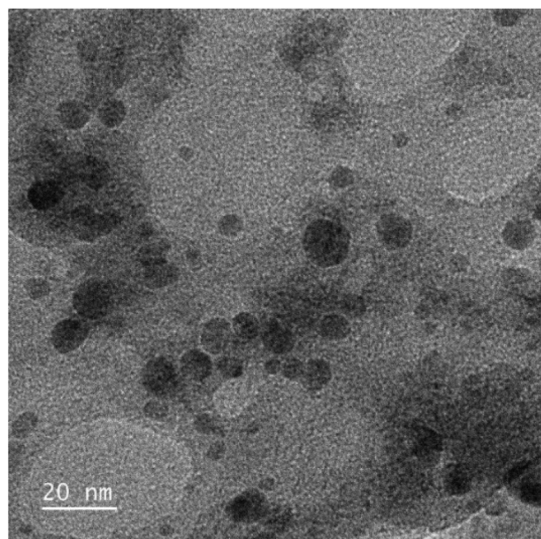**Fig. 3** SEM images of (a) blank calcium alginate NPs and (b) ferrous and folic acid loaded calcium alginate NPs.

Fig. 4 The TEM image of ferrous and folic acid loaded calcium alginate nanoparticles.

3.3.3.   Energy-dispersive X-ray spectroscopy (EDX). An EDX spectrometer was used to confirm the elements present in the NP matrix. The EDX spectra of the alginate NPs revealed that
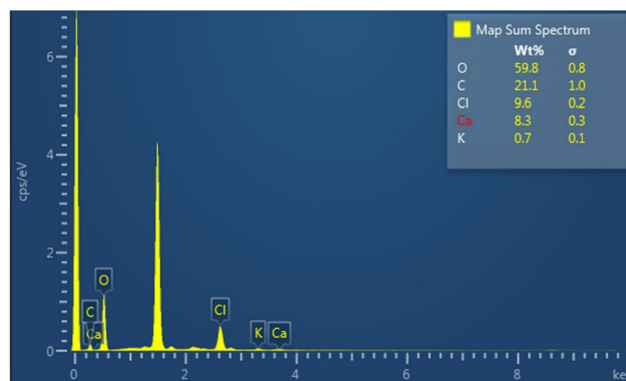

Fig. 5 EDX spectrum and elemental atomic percentages of Fe/folic loaded calcium cross-linked alginate nanoparticles.

the alginate NPs contain C, O, Ca and Cl present in the calcium alginate sample (Fig. 5) as primary elements. This confirms the successful replacement of sodium by calcium during the synthesis of calcium alginate NPs.

3.3.4.   Electron energy loss spectroscopy (EELS). Electron energy loss spectroscopy (EELS) analysis was performed to confirm the encapsulation of ferrous ascorbate and folic acid into the alginate NPs. Peaks present in the EELS spectrum (Fig. 6) confirmed the presence of encapsulated folic acid in the folic acid loaded alginate NPs as well as the cross-linker ions.

3.3.5.   Fourier transform infrared spectroscopy analysis. Polyelectrolyte complex interactions were observed to examine the relationship between the matrix components of the NPs and the encapsulated compounds. The nanoparticle system has been well established where the carboxyl group (COO–) of the alginate may interact with the cross-linker and form a complex between the two components. Changes in the FT-IR spectra in the absorption bands of the carboxyl groups were monitored. Analysis of FT-IR spectra for pure sodium alginate, blank calcium cross-linked alginate NPs and ferrous ascorbate and folic acid loaded calcium alginate NPs are shown in Fig. 7. The transmittance bands at 3234 cm^{-1} and 1593 cm^{-1} present in the spectrum of sodium alginate were assigned to the hydroxyl (OH) group and the asymmetric stretching peak of carboxylate salt (COO–), respectively. The absorption band at 1028 cm^{-1} is caused by the C–O–C stretching vibration of the glycosidic linkages of the sodium alginate polymer.

The peak attributed to stretching vibrations of –OH (3234 cm^{-1}) in sodium alginate powder was shifted to 3251–3257 cm^{-1} in calcium cross-linked ferrous ascorbate and folic acid loaded alginate NPs. The peak appearing at 1593 cm^{-1}, assigned to the stretching vibrations of the carboxyl group in sodium alginate, was shifted to 1622 cm^{-1} (Table 5) due to the displacement of sodium ions by calcium ions, thus changing the electron density of the carboxyl group in alginate.[26] The FT-IR spectra of blank alginate and ferrous ascorbate–folic acid loaded alginate NPs look similar, indicating that ferrous ascorbate and folic acid are encapsulated inside the alginate NPs.
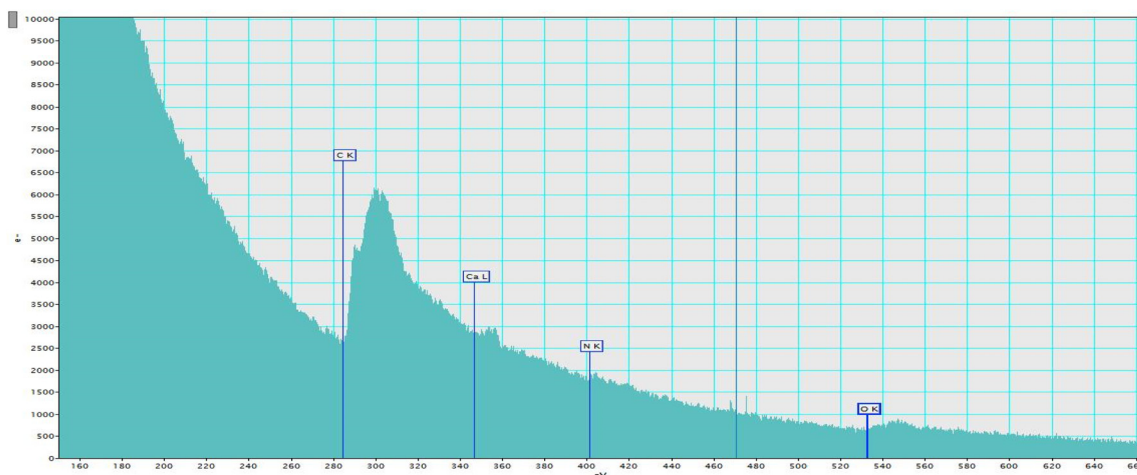
Fig. 6 EELS spectrum of Fe/folic acid loaded calcium cross-linked alginate nanoparticles.
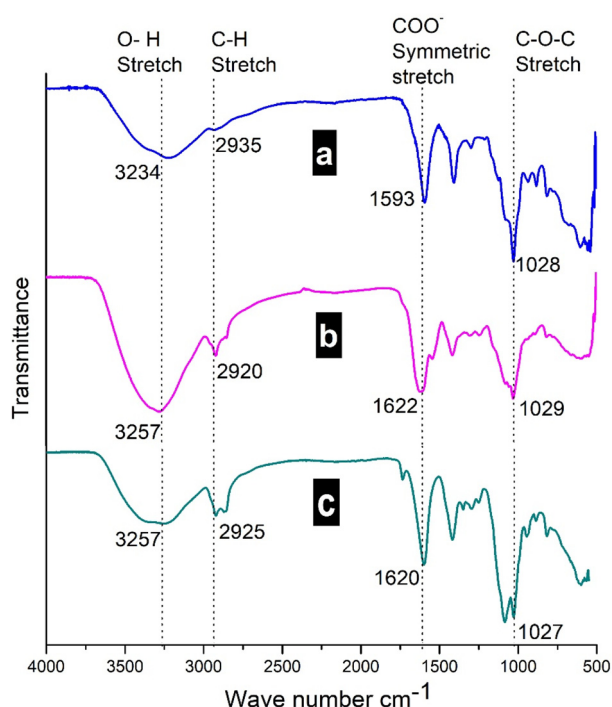

Fig. 7 FT-IR spectra of (a) sodium alginate, (b) calcium alginate, and (c) ferrous and folic acid loaded calcium alginate nanoparticles.

The encapsulation of ferrous and folic acid into NPs was investigated by FT-IR analysis. Pure folic acid displayed sharp peaks around 1652 cm^{-1} and 1411 cm^{-1} and those were overlapped with the IR absorption bands of the alginate NPs. However, the intensities of the absorption bands in the ferrous ascorbate and folic acid loaded alginate NPs are increased with slight shifts due to the interactions between the polymer and the ferrous ascorbate and folic acid.[27] These results indicate that ferrous ascorbate and folic acid were incorporated into the alginate polymeric network.

3.3.6. X-ray photoelectron spectroscopy analysis. XPS survey spectra of sodium alginate (Fig. 8) revealed the presence of sodium (1072.03 eV), carbon (287.03 eV) and oxygen (533.03 eV), with atomic percentages of 5.6%, 55.7% and 39.2%, respectively (Table 6). The oxygen-to-sodium ratio obtained from the XPS survey scan of sodium alginate was found to be 7, which is closely related to the theoretical value of 6.[28] XPS survey spectra of ferrous ascorbate and folic acid loaded calcium alginate NPs (Fig. 9, Table 7) revealed the displacement of the sodium ion with the respective cross-linker in stoichiometric proportion.

In the C 1s narrow scan of sodium alginate, calcium cross-linked alginate NPs (Fig. 10) displayed a peak that contained four peaks with the curve fit, related to the bonds at 284.9 eV (C–C), 286.4 eV (C–O), 288 eV (C–O–C), and 289.7 eV

Table 5 Diagnostic FT-IR assigned peaks for alginate nanoparticles

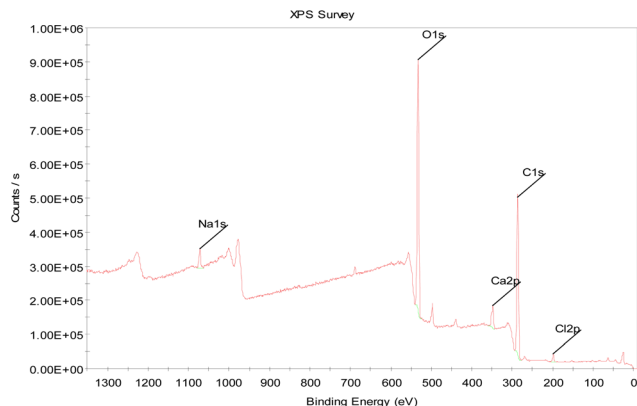| Functional groups in sodium alginate	Band position in sodium alginate (cm^{-1})	The shift in blank Ca alginate NPs (cm^{-1})	The shift in Fe/FA loaded Ca alginate NPs (cm^{-1})
Hydroxyl (OH) Stretch	3234	3257	3257
Alkyl (C–H) stretching	2935	2920	2925
Asymmetric stretching (COO$^-$)	1593	1622	1620
Symmetric stretching (COO$^-$)	1407	1419	1417
C–O–C stretching	1028	1029	1027

Fig. 8 XPS survey spectrum of sodium alginate.

Table 6 Atomic percentages of the elements present in sodium alginate

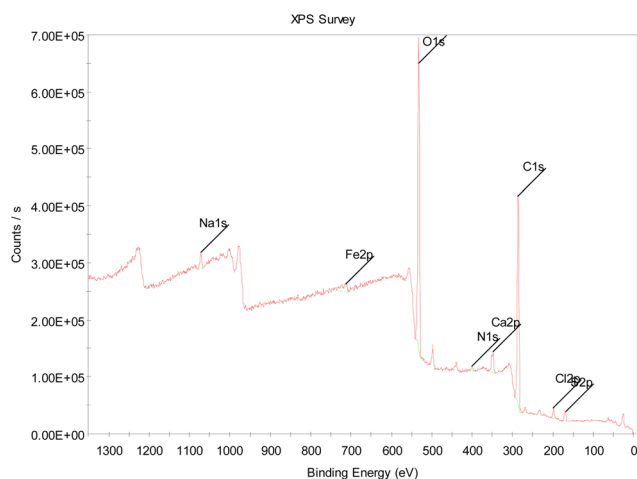| Element name and oxidative state	Atomic percentage (%)
C 1s	55.7
O 1s	39.2
Na 1s	5.1

Fig. 9 XPS survey spectrum of ferrous and folic acid loaded calcium alginate nanoparticles.

(COOH).[29] Sodium ions of the alginate were replaced by the Ca ions while preparing the NPs, resulting in a change in electron density. Due to this, the C 1s binding energy related to the C=O (289.7 eV) shifted to higher binding energy values. The ratio of intensities of C 1s binding energies related to the C–C and the C–O bond energies were relatively similar when compared to alginate. The C 1s narrow scan for ferrous ascorbate and folic acid loaded alginate NPs present distinct differences to that of the sodium alginate. The binding energy intensity of the C–C bond, relative to the C–O bond, was reduced, indicating that folic acid and ferrous ascorbate were successfully encapsulated into the NPs.

Table 7 Atomic percentages of the elements in ferrous/folic acid loaded calcium alginate nanoparticles

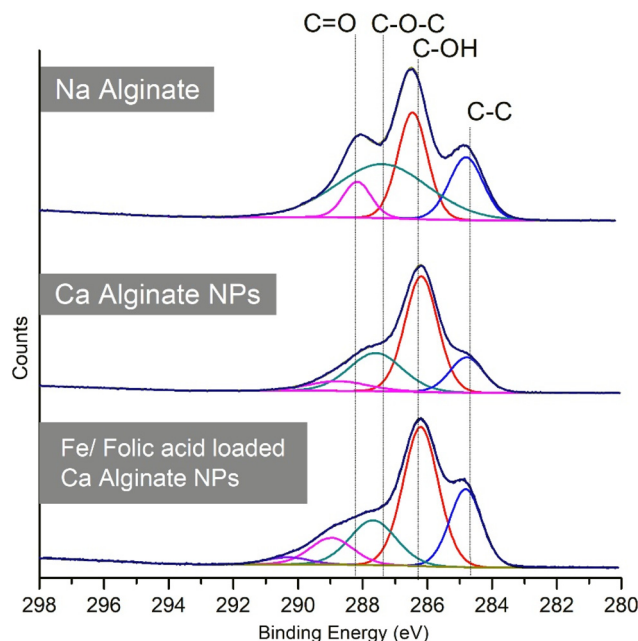| Element name and oxidative state	Fe/folic acid loaded calcium alginate NPs
C 1s	59.9
O 1s	33.0
Cl 2p	1.1
Na 1s	1.0
Ca 2p	1.5
Fe 2p	0.8
N 1s	1.3

Fig. 10 XPS carbon spectra of alginate nanoparticles.

In the Na and Ca narrow scan of sodium alginate, calcium cross-linked alginate NPs (Fig. 11) show peaks related to the O–Na (1071.8 eV), and O–Ca (347.3 eV) bonds,[28,30] which confirm the replacement of Na ions with Ca ions, due to the cross-linking of alginate polymer during the NP synthesis.

XPS analysis was performed to determine the elemental composition encapsulated in the alginate NPs. The narrow scan for the iron and nitrogen in ferrous ascorbate and folic acid encapsulated calcium alginate NPs is shown in Fig. 12. This XPS spectrum presents a characteristic peak for Fe ($2P_{3/2}$) with a peak maximum of 710.18 eV and a characteristic peak for Fe ($2P_{1/2}$) with a peak maximum of 723.7 eV.[31] XPS results have confirmed the encapsulation of ferrous ascorbate into alginate NPs without oxidation into its ferric form as shown previously in our laboratory.[18] Besides, encapsulated iron was observed to be stable for a few weeks. Folic acid contains nitrogen, and the XPS spectrum presents a characteristic peak at 400 eV produced by the nitrogen in the C–N bond.[32] This confirmed the successful encapsulation of folic acid into the alginate NPs.
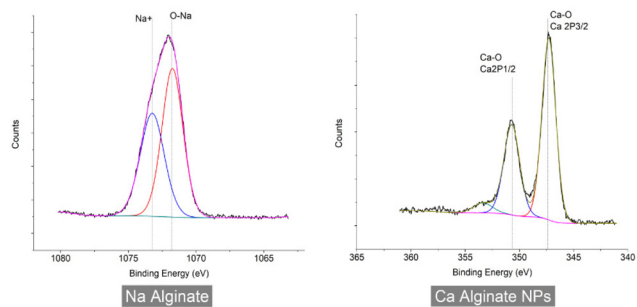
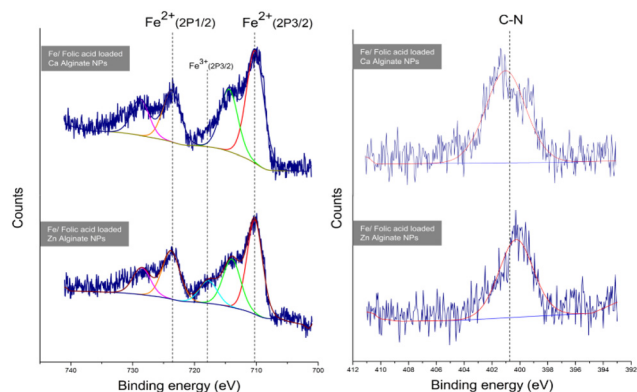**Fig. 11** XPS spectra for sodium alginate and calcium alginate nanoparticles.

Fig. 12 XPS spectra of iron and nitrogen in ferrous and folic acid loaded alginate nanoparticles.
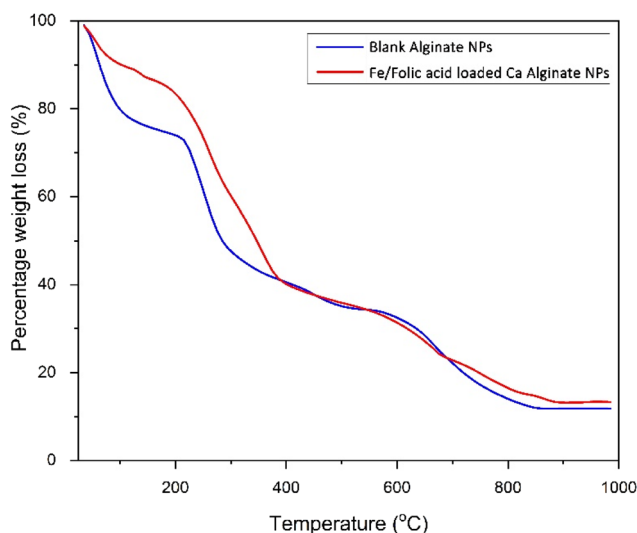

Fig. 13 Thermal decomposition of blank alginate nanoparticles and ferrous and folic acid loaded alginate nanoparticles.

3.3.7. Thermogravimetric analysis. The thermal decomposition of both blank alginate NPs and ferrous ascorbate–folic acid loaded alginate NPs (Fig. 13) showed the first mass loss with peaks at 62 °C and 75 °C, respectively, which could be attributed to the desorption of water. The second mass loss of 45% on the thermal decomposition of ferrous ascorbate and folic acid loaded alginate NPs was observed at 200–385 °C. The second mass loss (35%) of blank alginate NPs took place at a higher rate in the range of 240–350 °C. A minor mass loss (10%) between 400 °C and 500 °C was observed in the blank alginate NPs. A third mass loss (20%) between 600 °C and 1000 °C in ferrous ascorbate–folic acid loaded alginate NPs could be ascribed to the decomposition of encapsulated folic acid. A residue of 15% remained after completion of the Thermogravimetric analysis of ferrous and folic acid loaded alginate NPs because of the remaining metal ions.

3.4. Encapsulation efficiency and drug loading capacity

The percentage of successfully encapsulated ferrous ascorbate and folic acid into the NPs was determined using inductive coupled plasma mass spectroscopy and UV-visible spectrophotometry. Samples were analysed in triplicate, and the average encapsulation efficiency percentage of the optimized calcium alginate NPs was found to be 95% for ferrous ascorbate and 80% for folic acid.

The encapsulation efficiency of the alginate NPs was reduced when increasing the cross-linker concentration when the solution became acidic (low pH). The encapsulation efficiency for ferrous ascorbate was greater than 90% and increased with increasing ferrous sulphate concentration. The encapsulation efficiency for folic acid was greater than 80% (Table 8).

The drug loading capacity of the ferrous and folic acid in optimized calcium alginate NPs is summarized in Table 8. According to the results, the maximum loading capacity for the ferrous ascorbate was 3.2% and that of folic acid was 2.0% in calcium alginate NPs. These percentages reflect the amount of ferrous and folic acid encapsulated per unit amount of NPs.

3.5. *In vitro* release behaviour of ferrous ascorbate/folic acid loaded alginate nanoparticles

The release profile of ferrous ascorbate and folic acid from calcium alginate NPs at different pH values (at 37 ± 0.5 °C) was observed in this study. Release kinetics influenced the release of encapsulated ferrous ascorbate and folic acid from alginate nanoparticles using a 3000 kDa dialysis membrane. This semi-permeable barrier, with its specific molecular weight cut-off, allowed controlled diffusion of the released molecules (ferrous ascorbate and folic acid) while retaining the larger alginate

Table 8 Summary of encapsulation efficiency and drug-loading capacity of ferrous and folic acid in alginate nanoparticles at pH 6 ($n = 3$, $\pm$SEM)

	Fe/folic acid loaded calcium alginate nanoparticles	
	Ferrous ascorbate	Folic acid
EE (%)	$95 \pm 1.9\%$	$80 \pm 0.7\%$
LC (%)	$3.2 \pm 0.0\%$	$2.0 \pm 0.7\%$

nanoparticles within the sac. This configuration effectively mimicked their release profile in a simulated intestinal environment, mirroring the selective permeability of the intestinal epithelium. During the experiment, the dialysis sac containing the nanoparticles was immersed in a buffer solution, and the concentrations of released ferrous ascorbate and folic acid were monitored over time. This provided valuable insights into the diffusion kinetics and potential factors influencing the release profile.

The release study was performed for 3.5 h at pH 2 followed by 6 h at pH 7.4. According to Fig. 14, folic acid showed a burst release from the calcium cross-linked alginate NPs at pH 2 during the first 2 hours and reached equilibrium. Thereafter, a plateau was observed with no release up to 3.5 h in the acidic medium. When the pH was changed to pH 7.4, 20% of folic acid was released from calcium alginate NPs during the initial burst release phase within the first 1.5 hours followed by 23% of folic acid release in the next 4.5 h (during the 6 hours at pH 7.4). Thus, only 27% folic acid was released at pH 2, while 43% was released at pH 7.4, making a total of 70% folic acid released from calcium alginate NPs within 9.5 hours of release.

On the other hand, 18% of ferrous ascorbate was released from calcium alginate NPs within 3.5 hours at pH 2. According to Fig. 14, an initial burst release of ferrous ascorbate was observed in the first 2 hours followed by a slight increase up to 3.5 hours. However, by changing to pH 7.4 buffer, the release profile of ferrous ascorbate displayed an initial burst release of 12% of ferrous ions followed by sustained release of 7% of ferrous ions during the phase of 6 hours. Thus, a total of 19% of ferrous ions was released at pH 7.4, increasing the total of ferrous ascorbate released during the 9.5 h to 37%.

The initial burst release phase for ferrous ascorbate and folic acid indicates that a significant amount of ferrous ascorbate and folic acid associated with alginate NPs remained close to the surface with weak interaction forces between the polyelectrolyte complex and ferrous ascorbate/folic acid. These ferrous ions and folic acid were displaced rapidly within the alginate NP surface. The ferrous ascorbate and folic acid encapsulated within the matrix would face an additional physical barrier and take a longer period to release from the alginate NPs.

The release of ferrous ascorbate and folic acid from alginate NPs in the medium at pH 7.4 was much higher than that for the NPs in the medium at pH 2 over the same period. Alginate forms a compact acid-gel structure at low gastric pH conditions that restricts the release of drugs from the matrix of the NPs.[33] The pK_a is another important factor of the structural changes of alginate with the changes in pH of the medium. Thus, alginate having a pK_a of 3.4 remains undissociated and protects the encapsulated drug in a highly acidic medium.[18,33] This suggests that the ferrous ascorbate and folic acid release from ferrous ascorbate and folic acid loaded alginate NPs are pH sensitive and more of the drugs will be released into the blood circulation after cell internalization (blood pH is 7.4) than in the acidic stomach. Therefore, more drugs will be absorbed and transported to the site of action more efficiently than the commercially available folic acid and ferrous sulphate in tablets, which are not encapsulated. This drug delivery system will take around 20 hours to completely release all the drugs indicated by the extrapolation of the graph at pH 7.4 while considering the same steady-state release.

3.6. Release kinetics

The release kinetics of folic acid from ferrous ascorbate and folic acid loaded alginate NPs was assessed by kinetic modelling. The results are illustrated in Table 9. The release kinetics of ferrous ascorbate from ferrous ascorbate and folic acid loaded alginate NPs was also assessed by kinetic modelling. The results are illustrated in Table 10.

A drug release kinetics study was performed using the mathematical model of drug release, which describes the drug-releasing behaviour of pharmaceutical drug delivery systems. The best model fitting the release behaviour of ferrous ascorbate and folic acid from alginate NPs at pH 2 and pH 7.4 buffer solutions was selected based on the calculated r^2 values.

According to the adjusted r^2 values of the ferrous ascorbate and folic acid release from calcium alginate NPs, the initial burst release phase at pH 2 of folic acid release and ferrous ascorbate release followed the zero-order model and the first-order kinetics model, respectively. The sustained release phase of ferrous and folic acid release from calcium alginate NPs at pH 2 followed first-order kinetics, while the overall release followed Korsmeyer–Peppas kinetics. Folic acid release and ferrous ascorbate release from calcium alginate NPs at pH 7.4 followed zero-order kinetics, while the overall release followed the Korsmeyer–Peppas model.

Zero-order release kinetics depends on the concentration of the substrate, while the first-order release is characterized by
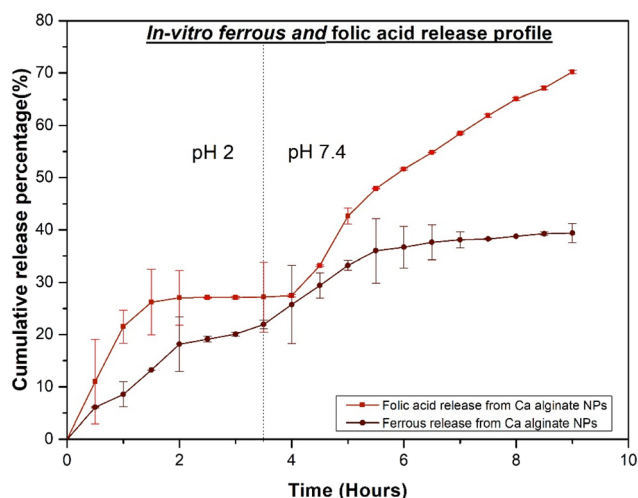

Fig. 14 Cumulative release of ferrous and folic acid from ferrous and folic acid loaded calcium alginate nanoparticles at predetermined time intervals in pH 2 and pH 7.4.

Table 9 Release kinetics of folic acid released from calcium alginate nanoparticles

Kinetics model	pH 2			pH 7.4		
	Burst release phase r^2	Sustained release phase r^2	Overall release r^2	Burst release phase r^2	Sustained release phase r^2	Overall release r^2
Zero-order	0.9719	0.8699	0.6897	0.9875	0.9949	0.9589
First-order	0.9098	0.8702	0.5464	0.9827	0.9883	0.8931
Hixson–Crowell	0.7997	0.8701	0.5119	0.9852	0.9902	0.9184
Higuchi	0.8696	0.8700	0.5767	0.9861	0.9920	0.9298
Korsmeyer–Peppas	0.9146	0.5701	0.9274	0.9585	0.9839	0.9707
(n)	0.33			0.69		

Table 10 Release kinetics of ferrous released from calcium alginate nanoparticles

Kinetic model	pH 2			pH 7.4		
	Burst release phase r^2	Sustained release phase r^2	Overall release r^2	Burst release phase r^2	Sustained release phase r^2	Overall release r^2
Zero-order	0.9875	0.9682	0.9382	0.9951	0.9684	0.7717
First-order	0.9964	0.9772	0.8721	0.9880	0.9651	0.7299
Hixson–Crowell	0.7805	0.9744	0.6778	0.9908	0.9662	0.7441
Higuchi	0.8776	0.9729	0.7914	0.9921	0.9668	0.7511
Korsmeyer–Peppas	0.9675	0.8897	0.9780	0.9044	0.9275	0.8250
(n)	0.65			0.39		

the release behaviour independent of the concentration of components. The Higuchi model for drug release behaviour represents the drug release by diffusion while the Korsmeyer–Peppas model represents the release of entrapped ferrous ascorbate and folic acid from alginate NPs due to polymer relaxation and diffusion.[34]

According to the results obtained from ferrous ascorbate and folic acid release behaviour in these kinetics models, the mechanism that best describes the release of ferrous ascorbate and folic acid from calcium alginate NPs can be explained by the value of the release exponent (n) (Table 11).

According to the calculated release exponent for folic acid release from calcium alginate NPs, the release mechanism at pH 2 (n = 0.33) and ferrous ascorbate release at pH 7.4 (n = 0.40) followed Less Fickian diffusion, while the folic acid release at pH 7.4 and ferrous ascorbate release mechanism at pH 2 can be suggested as non-Fickian anomalous diffusion

processes with the release exponent being 0.69 and 0.65, respectively. For spherical particles, $n > 0.43$ indicates a Fickian diffusion characterized by the high velocity of solvent diffusion into the interior of the NP matrix and the low velocity of polymeric relaxation. However, $0.43 < n < 0.85$ indicates a non-Fickian anomalous release.

An anomalous release mechanism corresponds to polymer hydration, solvent penetration, drug dissolution and polymer erosion, which determines the drug release from hydrophilic polymer materials.[36,37]

4. Conclusions

An alginate nanoparticle was successfully prepared by loading ferrous ascorbate and folic acid using a modified ionic gelation method with a dripping technique. The nanoparticles were characterized by various techniques, such as SEM, TEM, XPS, EELS, and FT-IR, which confirmed their size, shape, morphology, and composition. The nanoparticles showed high encapsulation efficiency and loading capacity of both iron and folate, as well as good stability and slow-release behaviour at different pH conditions. The release mechanism of iron and folate from the nanoparticles followed the Korsmeyer–Peppas diffusion model, with some variations depending on the pH and the type of element. The nanoparticles could protect iron and folate from degradation and interaction with other substances in the gastrointestinal tract, as well as reduce the side effects and toxicity associated with high doses of these elements. The nanoparticles could also enhance the bio-

Table 11 Diffusional exponent (n) values and release transport mechanisms based on spherical shape vehicles[35]

Diffusional exponent (n) for spherical shape particles	Release mechanism
$n < 0.43$	Less Fickian
$n = 0.43$	Fickian diffusion
$0.43 < n < 0.85$	Anomalous transport
$n = 0.85$	Case II transport
$n > 0.85$	Super case II transport

availability and patient adherence to iron and folate, which are both important for preventing anaemia and other health problems. The nanoparticles could be a potential oral delivery system for iron and folate, especially for pregnant women and children, who are more vulnerable to deficiency. Future studies should evaluate the *in vivo* performance and efficacy of the nanoparticles in animal models and human subjects.

Author contributions

All authors contributed to the study conceptualization. Investigation, formal analysis, data curation, software, visualization, and writing – original draft were by Weranga Rajapaksha. Tharanga Thoradeniya, D. N. Karunaratne and V. Karunaratne were engaged in writing – review & editing and supervision.

Conflicts of interest

There are no conflicts to declare.

Acknowledgements

References

1 M. D. R. Islam, S. Akash, M. H. Jony, M. D. N. Alam, F. T. Nowrin, M. D. M. Rahman, *et al.*, Exploring the potential function of trace elements in human health: a therapeutic perspective, *Mol. Cell. Biochem.*, 2023, **478**(10), 2141–2171.

2 S. B. Kumar, S. R. Arnipalli, P. Mehta, S. Carrau and O. Ziouzenkova, Iron Deficiency Anemia: Efficacy and Limitations of Nutritional and Comprehensive Mitigation Strategies, *Nutrients*, 2022, **14**(14), 2976.

3 R. Obeid, K. Oexle, A. Rißmann, K. Pietrzik and B. Koletzko, Folate status and health: challenges and opportunities, *J. Perinat. Med.*, 2016, **44**(3), 261–268.

4 A. C. Antony, R. M. Vora and S. J. Karmarkar, The silent tragic reality of Hidden Hunger, anaemia, and neural-tube defects (NTDs) in India, *Lancet Reg. Health – Southeast Asia*, 2022, **6**, 100071.

5 G. H. Tang and M. Sholzberg, Iron deficiency anemia among women: An issue of health equity, *Blood Rev.*, 2023, 101159.

6 N. Milman, Intestinal absorption of folic acid - new physiologic & molecular aspects, *Indian J. Med. Res.*, 2012, **136**(5), 725–728.

7 T. Ems, K. St Lucia and M. R. Huecker, Biochemistry, in *Iron Absorption*, ed. StatPearls, StatPearls Publishing, Treasure Island (FL), 2023.

8 C. Xu, Q. Ban, W. Wang, J. Hou and Z. Jiang, Novel nano-encapsulated probiotic agents: Encapsulate materials, delivery, and encapsulation systems, *J. Controlled Release*, 2022, **349**, 184–205.

9 Y. G. Seo, D. H. Kim, T. Ramasamy, J. H. Kim, N. Marasini, Y. K. Oh, *et al.*, Development of docetaxel-loaded solid self-nanoemulsifying drug delivery system (SNEDDS) for enhanced chemotherapeutic effect, *Int. J. Pharm.*, 2013, **452**(1), 412–420.

10 K. Vyas, M. Rathod and M. M. Patel, Insight on nano drug delivery systems with targeted therapy in treatment of oral cancer, *Nanomedicine*, 2023, **49**, 102662.

11 A. Pillai, D. Bhande and V. Pardhi, Controlled Drug Delivery System, in *Advanced Drug Delivery: Methods and Applications*, ed. T. S. Santra and A. U. S. Shinde, Springer Nature, Singapore, 2023, pp. 267–289. (Studies in Mechanobiology, Tissue Engineering and Biomaterials). Available from: DOI: 10.1007/978-981-99-6564-9_11.

12 N. Kamaly, B. Yameen, J. Wu and O. C. Farokhzad, Degradable Controlled-Release Polymers and Polymeric Nanoparticles: Mechanisms of Controlling Drug Release, *Chem. Rev.*, 2016, **116**(4), 2602–2663.

13 D. Kothale, U. Verma, N. Dewangan, P. Jana, A. Jain and D. Jain, Alginate as Promising Natural Polymer for Pharmaceutical, Food, and Biomedical Applications, *Curr. Drug Delivery*, 2020, **17**(9), 755–775.

14 M. A. Taemeh, A. Shiravandi, M. A. Korayem and H. Daemi, Fabrication challenges and trends in biomedical applications of alginate electrospun nanofibers, *Carbohydr. Polym.*, 2020, **228**, 115419.

15 C. Hu, W. Lu, A. Mata, K. Nishinari and Y. Fang, Ions-induced gelation of alginate: Mechanisms and applications, *Int. J. Biol. Macromol.*, 2021, **177**, 578–588.

16 M. B. Łabowska, M. Skrodzka, H. Sicińska, I. Michalak and J. Detyna, Influence of Cross-Linking Conditions on Drying Kinetics of Alginate Hydrogel, *Gels*, 2023, **9**(1), 63.

17 N. Samiraninezhad, K. Asadi, H. Rezazadeh and A. Gholami, Using chitosan, hyaluronic acid, alginate, and gelatin-based smart biological hydrogels for drug delivery in oral mucosal lesions: A review, *Int. J. Biol. Macromol.*, 2023, **252**, 126573.

18 N. P. Katuwavila, A. D. L. C. Perera, D. Dahanayake, V. Karunaratne, G. A. J. Amaratunga and D. N. Karunaratne, Alginate nanoparticles protect ferrous from oxidation: Potential iron delivery system, *Int. J. Pharm.*, 2016, **513**(1), 404–409.

19 G. Pamunuwa, N. Anjalee, D. Kukulewa, C. Edirisinghe, F. Shakoor and D. N. Karunaratne, Tailoring of release properties of folic acid encapsulated nanoparticles via changing alginate and pectin composition in the matrix, *Carbohydr. Polym. Technol. Appl.*, 2020, **1**, 100008.

20 D. Massella, E. Celasco, F. Salaün, A. Ferri and A. A. Barresi, Overcoming the Limits of Flash Nanoprecipitation: Effective Loading of Hydrophilic Drug into Polymeric Nanoparticles with Controlled Structure, *Polymers*, 2018, **10**(10), 1092.

21 J. Siepmann and N. A. Peppas, Modeling of drug release from delivery systems based on hydroxypropyl methyl-cellulose (HPMC), *Adv. Drug Delivery Rev.*, 2001, **48**(2–3), 139–157.

22 N. Hoshyar, S. Gray, H. Han and G. Bao, The effect of nanoparticle size on in vivo pharmacokinetics and cellular interaction, *Nanomedicine*, 2016, **11**(6), 673–692.

23 N. L. Francis, P. M. Hunger, A. E. Donius, B. W. Riblett, A. Zavaliangos, U. G. K. Wegst, *et al.*, An ice-templated, linearly aligned chitosan-alginate scaffold for neural tissue engineering, *J. Biomed. Mater. Res., Part A*, 2013, **101**(12), 3493–3503.

24 S. N. Pawar and K. J. Edgar, Alginate derivatization: A review of chemistry, properties and applications, *Biomaterials*, 2012, **33**(11), 3279–3305.

25 J. J. Chuang, Y. Y. Huang, S. H. Lo, T. F. Hsu, W. Y. Huang, S. L. Huang, *et al.*, *Int. J. Polym. Sci.*, 2017, **2017**, e3902704.

26 H. Daemi and M. Barikani, Synthesis and characterization of calcium alginate nanoparticles, sodium homopolymannuronate salt and its calcium nanoparticles, *Sci. Iran.*, 2012, **19**(6), 2023–2028.

27 S. R. Abulateefeh, M. A. Khanfar, R. Z. A. Bakain and M. O. Taha, Synthesis and characterization of new derivatives of alginic acid and evaluation of their iron(III)-crosslinked beads as potential controlled release matrices, *Pharm. Dev. Technol.*, 2014, **19**(7), 856–867.

28 A. Jejurikar, X. T. Seow, G. Lawrie, D. Martin, A. Jayakrishnan and L. Grøndahl, Degradable alginate hydrogels crosslinked by the macromolecular crosslinker alginate dialdehyde, *J. Mater. Chem.*, 2012, **22**(19), 9751.

29 K. Jradi, C. Maury and C. Daneault, Contribution of TEMPO-Oxidized Cellulose Gel in the Formation of Flower-Like Zinc Oxide Superstructures: Characterization of the TOCgel/ZnO Composite Films, *Appl. Sci.*, 2015, **5**(4), 1164–1183.

30 Z. Tong, Y. Chen, Y. Liu, L. Tong, J. Chu, K. Xiao, *et al.*, Preparation, Characterization and Properties of Alginate/Poly(γ-glutamic acid) Composite Microparticles, *Mar. Drugs*, 2017, **15**(4), 91.

31 M. C. Biesinger, B. P. Payne, A. P. Grosvenor, L. W. M. Lau, A. R. Gerson and R. S. T. C. Smart, Resolving surface chemical states in XPS analysis of first row transition metals, oxides and hydroxides: Cr, Mn, Fe, Co and Ni, *Appl. Surf. Sci.*, 2011, **257**(7), 2717–2730.

32 C. Tudisco, M. T. Cambria, A. E. Giuffrida, F. Sinatra, C. D. Anfuso, G. Lupo, *et al.*, Comparison Between Folic Acid and gH625 Peptide-Based Functionalization of Fe3O4 Magnetic Nanoparticles for Enhanced Cell Internalization, *Nanoscale Res. Lett.*, 2018, **13**, 45.

33 S. Goswami, J. Bajpai and A. K. Bajpai, Calcium alginate nanocarriers as possible vehicles for oral delivery of insulin, *J. Exp. Nanosci.*, 2014, **9**(4), 337–356.

34 C. M. Klech and A. P. Simonelli, Examination of the moving boundaries associated with non-Fickian water swelling of glassy gelatin beads: Effect of solution pH, *J. Membr. Sci.*, 1989, **43**(1), 87–101.

35 N. A. Peppas and J. J. Sahlin, A simple equation for the description of solute release. III. Coupling of diffusion and relaxation, *Int. J. Pharm.*, 1989, **57**(2), 169–172.

36 L. Keawchaoon and R. Yoksan, Preparation, characterization and in vitro release study of carvacrol-loaded chitosan nanoparticles, *Colloids Surf., B*, 2011, **84**(1), 163–171.

37 M. L. Bruschi, editor. 5 - Mathematical models of drug release, in *Strategies to Modify the Drug Release from Pharmaceutical Systems*, Woodhead Publishing, 2015, pp. 63–86.